Excising das All: Evolving Maxwell waves beyond Scri

James R. van Meter
Laboratory for Gravitational Astrophysics, NASA Goddard Space Flight Center, Greenbelt, Maryland 20771

David R. Fiske
Intelligent Systems Division, Decisive Analytics Corporation, 1235 South Clark Street, Arlington, Virigina 22202 and
Laboratory for Gravitational Astrophysics, NASA Goddard Space Flight Center, Greenbelt, Maryland 20771

Charles W. Misner
Department of Physics, University of Maryland, College Park, Maryland 20742-4111 and
Albert-Einstein-Institut, Max-Planck-Institut für Gravitationsphysik, Am Mühlenberg 1, D-14476 Potsdam, Germany
(Dated: 26 February 2006)

We study the numerical propagation of waves through future null infinity in a conformally compactified spacetime. We introduce an artificial cosmological constant, which allows us some control over the causal structure near null infinity. We exploit this freedom to ensure that all light cones are tilted outward in a region near null infinity, which allows us to impose excision-style boundary conditions in our finite difference code. In this preliminary study we consider electromagnetic waves propagating in a static, conformally compactified spacetime.

I. INTRODUCTION

The German noun "das All" refers to the Universe, but sometimes in a sense unfamiliar in English where it translates better as "outer space." A spacecraft, after launch, might be described as *entering* das All. In the computations reported here, it is precisely this outer space — the physical details far from a source of gravitational (or in our case electromagnetic) waves — which is excised from the computational model in analogy to the way the internal mysteries/singularities of a black hole are often excised in computational models. We develop and implement the proposals made earlier in Refs. [1–3] to obtain wave forms promptly at infinity by using hyperboloidal time slices in a Cauchy evolution, to avoid infinitesimal time steps through conformal compactification, to convert outer boundary conditions to excision boundary conditions by using an artificial cosmological constant, and to defend the physical domain against computational boundary errors by tilting the light cones further outward in the region beyond the outer horizon. The aim of this paper is to explore the application of this set of boundary treatment tools in a low cost application in order to see whether there are unexpected impediments to its application, and to get guidance for the best approaches for its application to larger problems.

The use of hyperboloidal slicings in numerical relativity has been carefully studied (e.g. Refs. [4–7]), and there are existing numerical results generated on compactified domains (e.g. Ref. [8]). This paper contributes to this literature by combining these two techniques in a spacetime with an artificial cosmological structure designed to make it easier to construct boundary conditions at $\mathscr{I}^+$, and by studying the effectiveness of modifying the light cone structure in the region of the analytically continued spacetime exterior to $\mathscr{I}^+$ to prevent non-physical, incoming radiation from piling up on the non-physical side of $\mathscr{I}^+$. That said, our approach to the problem does not require special modifications to the form of the differential equations solved to model the physical problem. It should be compatible with exisiting numerical codes desgined to solve the initial problem, described by some variant of the the Einstein equations in an Arnowitt-Desner-Misner 3+1 decomposition [9].

Our work is also complementary to community wide efforts to use mesh refinement techniques in numerical relativity. Several groups have recently and successfully incorporated mesh refinement techniques into their Einstein solvers (i.e. Refs. [8, 10–18]). This technology allows groups to push their computational boundaries to very large coordinate distances, reducing the effects of incoming radiation and constraint violating modes introduced by applying boundary conditions at a finite distance.

While mesh refinement has greatly increased the power of modern codes, it also has limitations. It is now fairly easy to surround a computational domain with coarser and coarser grids, but at some point the coarse grids cannot resolve a wavelength, see, e.g. Refs. [13] and [19, Section 4.3]. They can, however, insulate the active, wave generation regions of the computational domain from boundary problems for a limited period of time. During this period waveforms have been successfully extracted from inner regions as small as 2.4 wavelengths from the center [18]. The hyperboloidal slicings considered here and elsewhere have the advantage that they asymptote to the outgoing light cones in the spacetime. Outgoing waves, therefore, appear asymptotically constant and require very few points to resolve them all the way to $\mathscr{I}^+$.

The rest of the paper is organized as follows: In Section II, we biefly summarize the formalism we use in our code, both for the background spacetime metric and for the Maxwell equations themselves. In Section III we de-

scribe the numerical methods used to solve the equations. We summarize the numerical results and discuss the implications for future work in Section IV. Additional detail is provided in the Appendix.

II. FORMALISM

A. Spacetime Metric

As in Refs. [1, 2] the background metric for this study will be the de Sitter spacetime

$$ds^2 = -dT^2+dX^2+dY^2+dZ^2+(R^2/L^2)(dT-dR)^2 \quad (1)$$

with an artificial cosmological constant $\Lambda = +3/L^2$. We are interested in the limit $1/L^2 \to 0$ when this becomes Minkowski spacetime, and the cosmological constant is used to make boundary conditions numerically simpler (we hope) at the de Sitter horizon than they would be at flat spacetime's $\mathscr{I}^+$. The de Sitter horizon is the null hypersurface $R = L$ in this metric. As before we introduce the coordinate changes

$$\frac{T}{s} = u + \frac{r^2/2}{1-r^2/4} \quad (2a)$$

$$\frac{X^i}{s} = \frac{x^i}{1-r^2/4} \quad (2b)$$

as used in Refs. [1–3], where $R^2 = X^2+Y^2+Z^2 \equiv X^iX^i$ and $r^2 = x^2+y^2+z^2 \equiv x^ix^i$. This brings $\mathscr{I}^+$ in to $r = 2$ in the Minkowski case and in the de Sitter case makes this a spacelike hypersurface beyond the de Sitter horizon which is part of de Sitter spacetime's future causal boundary which is also called $\mathscr{I}^+$. The hypersurfaces of constant u are then hyperboloids

$$[T - s(u-1)]^2 - R^2 = s^2 \quad (3)$$

in Minkowski spacetime and are also asymptotically null spacelike hypersurfaces in the de Sitter modification. This leads to a metric which is singular at $r = 2$, but only in a conformal factor $s^2/q^2 = s^2/(1-r^2/4)^2$ which does not appear in the Maxwell equations. Thus we can drop this conformal factor and our test problem is to solve the Maxwell equations in the resultant metric which is of the form

$$ds^2 = -\alpha^2dt^2 + \gamma_{ij}(dx^i+\beta^idt)(dx^j+\beta^jdt) \quad (4)$$

with $t = u$. When we choose $W = 0$, the following equations give the analytically continued and conformally regulated de Sitter metric described above:

$$\alpha = \frac{(1-W)(1+\frac{r^2}{4})}{\sqrt{1+\left(\frac{sS}{L}\right)^2}} \quad (5a)$$

$$\beta^i = -x^i\frac{1-W+\left(\frac{s}{L}\right)^2 S}{1+\left(\frac{sS}{L}\right)^2} \quad (5b)$$

$$\gamma_{ij} = \left(\frac{sS}{Lr}\right)^2 x_ix_j + \delta_{ij} \quad (5c)$$

where

$$S = \frac{(1-W)r}{(1+\frac{r}{2})^2} + \frac{1}{4}\left(\frac{L}{s}\right)^2 W. \quad (6)$$

Figure 1 below shows the coordinate speeds for light rays on the inward side of the light cone $v_{\rm in}$, on the outward side of the light cone $v_{\rm out}$, and for a timelike center of the light cone $v_{\rm center} = -\beta$ normal to the time slices of constant u. Because this allows light rays to move inward

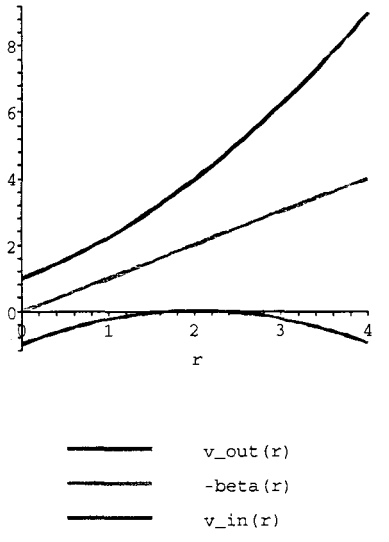

FIG. 1: Coordinate speeds for the de Sitter lightcone: inward ($v_{\rm in}$), normal to the spacelike time slices ($-\beta$), and outward ($v_{\rm out}$). For the Minkowski metric the graph looks very similar, except that $v_{\rm in}$ is there never positive.

($v_{\rm in} < 0$) in some of the region beyond $\mathscr{I}^+$ but within our computational grid, we choose instead to take

$$W(r) = \Theta(r-2)\frac{(r-2)^4}{\left[(r-2)^2+\frac{1}{2}\right]^2} \quad (7)$$

to be a smooth step function that modifies the metric beyond $r = 2$ in a way that keeps the "incoming" coordinate speed of light $v_{in} = dr/du$ positive (that is outgoing) when $r > 2$. The function W is a C^3 modification of $\Theta(r-2)$, the Heaviside step function that jumps from 0 to 1 at $r = 2$. Note that for $r \le 2$, this metric has the surprising property that the outgoing speed of light $v_{out} = (1+r/2)^2$ is independent of the cosmological constant paramter L (cf. equation 8 in Ref. [1]). Although in general the presence of a cosmological constant alters the causal structure of a spacetime, and indeed it does modfiy the ingoing radial speed of light in the present example, it does not change the outgoing radial speed of light from that of the original Minkowski spacetime. This fact will prove useful for numerical diagnostics. Figure 2 below shows the modified light cone directions in

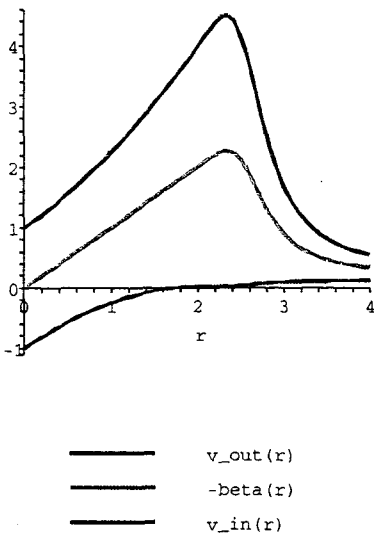

FIG. 2: Coordinate speeds for the modified de Sitter (eqn. 7) lightcone: inward light rays, ($v_{\rm in}$), motion normal to the spacelike time slices ($-\beta$), and outward light rays ($v_{\rm out}$).

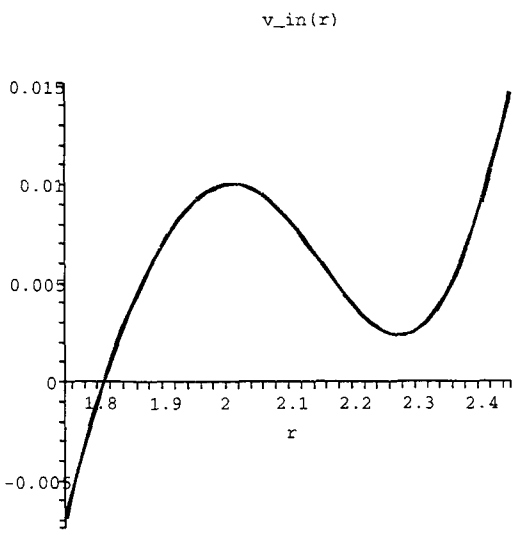

FIG. 3: Coordinate speeds inward ($v_{\rm in}$) for light rays in the modified (eqn. 7) de Sitter metric.

this case. For this modified de Sitter metric using equation (7) one finds very low inward light velocities in the region just outside $\mathscr{I}^+$ as seen in Fig. 3. This can lead to fields propagating along the inward side of the lightcone spending very long periods of time in the region $r \approx 2.3$ as illustrated by the world line of a light ray in Fig. 4.

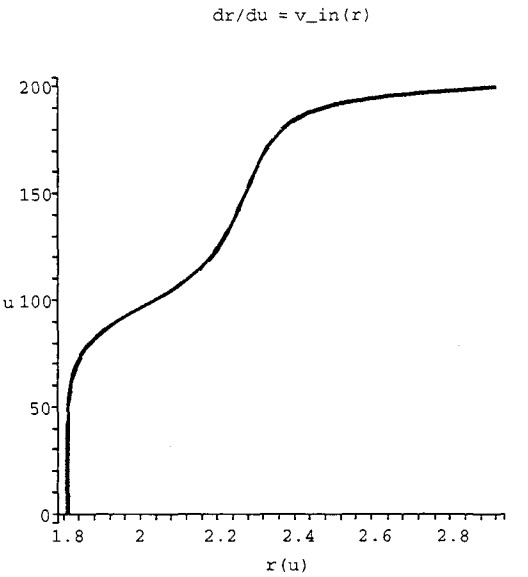

FIG. 4: World line of a light ray on the inward side of the light cone in the modified de Sitter metric.

B. Maxwell Equations

We take the Maxwell equations in the form given in the DeserFest paper [1]. The quantities involved are all various components of the usual 4-dimensional Maxwell fields $F_{\mu\nu}$ and $\mathcal{F}^{\mu\nu} = \sqrt{-g}g^{\mu\alpha}g^{\nu\beta}F_{\alpha\beta}$. In particular, for any $3+1$ metric of the form Eq. 4 we define,

$$\mathcal{F}^{0i} = \mathcal{D}^i \quad , \quad \mathcal{F}^{ij} = [ijk]H_k \tag{8a}$$

and

$$F_{i0} = E_i \quad , \quad F_{ij} = [ijk]\mathcal{B}^k \quad . \tag{8b}$$

Here $[ijk]$ is the completely antisymmetric symbol $[ijk] = 0, \pm 1$ with $[123] = +1$. The fundamental fields in the formulation are $\mathcal{B}^i$ and $\mathcal{D}^i$. The constraints read

$$\partial_i \mathcal{B}^i = 0 = \partial_i \mathcal{D}^i \quad . \tag{9}$$

These fields are each three dimensional vector densities so these equations are three dimensionally covariant. In terms of these primary fields, two auxiliary fields E_i and H_i are computed by the formulae

$$E_i = (\alpha/\sqrt{\gamma})\gamma_{ij}\mathcal{D}^j + [ijk]\beta^j\mathcal{B}^k \tag{10a}$$

and

$$H_i = (\alpha/\sqrt{\gamma})\gamma_{ij}\mathcal{B}^j - [ijk]\beta^j\mathcal{D}^k \quad . \tag{10b}$$

The evolution equations are then

$$\partial_0 \mathcal{B}^i = -[ijk]\partial_j E_k \tag{11a}$$

and

$$\partial_0 \mathcal{D}^i = [ijk]\partial_j H_k \quad . \tag{11b}$$

Note that the metric does not appear in equations (9) nor (11), and that the metric quantities which do appear in equations (10) are conformally invariant. This is a first order PDE system in flux conservation form.

C. Initial Data

For initial data and some testing purposes we have used the solution of the flat spacetime Maxwell equations employed by Knapp et al. [20] and subsequently by Fiske [21]. This solution is a wave pulse, which propagates smoothly from $\mathscr{I}^-$ through the origin and out to $\mathscr{I}^+$. It consists of a torroidal $\mathcal{D}$ field and a poloidal $\mathcal{B}$ field generated from a vector potential, described in Ref. [1],

$$A = A_i dX^i = f \sin^2\theta d\phi \tag{12}$$

where

$$\sin^2\theta d\phi = \frac{1}{R^2}\left(X dY = Y dX\right) = \frac{1}{r^2}\left(x dy - y dx\right) \tag{13}$$

and

$$f = \left(\frac{1}{R} - 2\lambda U\right) e^{-\lambda U^2} - \left(\frac{1}{R} + 2\lambda V\right) e^{-\lambda V^2}. \tag{14}$$

In these equations $U \equiv T - R$ and $V \equiv T + R$ are the Minkowski retarded and advanced times, which are then expressed in terms of the compactified coordinates u and r as $U/s = u - 2 + 2/(1+\frac{1}{2}r)$ and $V/s = u - 2 + 2/(1-\frac{1}{2}r)$. Finally, $\mathcal{B}^i$ and $\mathcal{D}^i$ are calculated by differentiating this A field. The term containing $e^{-\lambda V^2}$ can be smoothly omitted when $r > 2$ since all its derivatives vanish at $r = 2$, but the term with $e^{-\lambda U^2}$ must be retained to preserve the constraints, and we thus have nonzero initial data in the unphysical region $r > 2$, and did not have sufficient resolution to reduce the pulse width to make these unphysical data insignificant.

For all of the simulations described in this paper, we choose $\lambda = 1$ (or, equivalently, we measured distances in the uncompactified space in units of $\lambda^{-1/2}$). The pulse width is then $\lambda^{-1/2}$. We also always choose $s = 1$ to set the size of the region near the origin where the hyperboloidal slices are somewhat flat. Our results reported below used either $s/L = 0$ for the Minkowski case, or $s/L = 0.1$ for the de Sitter and modified (eqn. 7) de Sitter cases. Thus the r = const hypersurfaces were not spacelike for the de Sitter case when $r > 2.21$

III. NUMERICS

A key point in our approach to this problem is that we do not require special numerical techniques to handle the compactified spacetime at or within $\mathscr{I}^+$. At all interior points, we use second-order, finite-difference approximations to all derivatives. At the computational boundary beyond $\mathscr{I}^+$, we use a second-order, one-sided stencil for normal derivatives. We integrate forward in time using the iterated Crank-Nicholson method commonly used in numerical relativity codes [22].

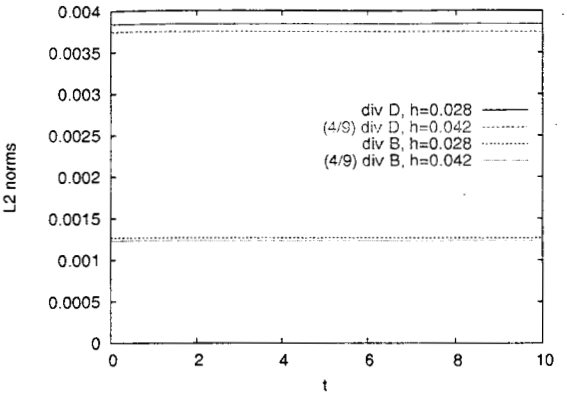

FIG. 5: The L2 norms (over the region $r \leq 2$) of the constraints plotted vs. time. The higher resolution data is multiplied by the factor appropriate to demonstrate second order convergence. The initial values arise from $\mathcal{B}$ and $\mathcal{D}$ fields which are exact analytic solutions of the constraints, evaluated at the grid points and then differenced to form the constraints.

Our decision to use one-sided differencing at the computational boundary was (in our view) the simplest thing to do. It turns out, however, to be equivalent to the black hole excision boundary conditions first studied in Ref. [23]. To be precise, along a normal to the boundary, the composition of third order extrapolation to a cell just outside the boundary (as used for excision) with second-order center differencing at a cell just inside the boundary gives the same stencil as second-order one-sided differencing at the cell just inside the boundary. This is consistent with our mental picture of excising a region exterior to $\mathscr{I}^+$, and reflects the similarity between $\mathscr{I}^+$ (at which all characteristics point outward) and an apparent horizon of a black hole (at which all characteristics point inward). As with black hole excision, it is critical for stable and accurate simulations that all light cones at the excision boundary tilt towards the excised region, hence the need for the beyond-$\mathscr{I}^+$ metric modification described in Section II A. Without these equation (7) modifications, the light cones would point outward only in a neighborhood of $\mathscr{I}^+$ which did not extend out to the computational boundary of the cubic grid enclosing $\mathscr{I}^+$.

We have verified that our code converges at second order accuracy throughout the physical domain. We paid special attention to the region in the vicinity of $\mathscr{I}^+$, and we are satisfied that the code coverges there as well. Figure 5 explicitly shows a two-point convergence test on the constraints over the physical region $r \leq 2$, which are seen to be second-order convergent to zero and nearly constant.

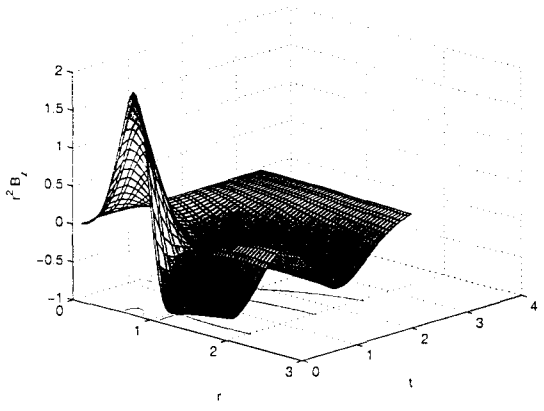

FIG. 6: A space-time graph of $r^2\mathcal{B}^z$. Notice that the wave passes through $\mathscr{I}^+$, located at $r = 2$ in our coordinate system.

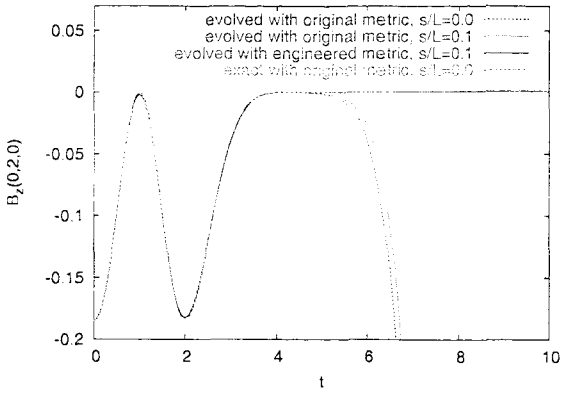

FIG. 7: The time evolution of $\mathcal{B}^z$ at a point on $\mathscr{I}^+$. We show both a numerical solution generated by our code using the modified de Sitter (engineered lightcones beyond $\mathscr{I}^+$) and the analytic solution with zero cosmological constant. The close agreement of the lines suggests that we are able to accurately capture the behavior of the fields as they pass through $\mathscr{I}^+$. Other numerical evolutions based on the original (compactified, analytically continued) Minkowski metric ($s/L = 0.0$) and the similiar de Sitter metric ($s/L = 0.1$), for which the grid boundaries were not spacelike, fail after $t \equiv u = 4$.

IV. RESULTS

When evolving with the original, conformal, de Sitter metric given in Eq. (1), large errors eventually appear near the computational grid boundary, grow exponentially in time, and propagate inside $\mathscr{I}^+$. This problem was slightly worse when the cosmological constant was omitted. These cataclysmic errors originated at the grid boundary which in these cases was not a spacelike hypersurface for which excisions (at apparent horizons) were designed. [The (correctly zero) field $\mathcal{B}^z$ took values near $10^{-3+5u/4}$ at the edges of the $z = 0$ plane after $u = 4$, and values 10^8 smaller at $\mathscr{I}^+$ for $4 < u < 20$.] As anticipated in Section II A we proceeded to artificially tilt the lightcones outwards beyond $\mathscr{I}^+$ to make the grid boundaries spacelike.

Figure 6 shows a space-time view of the z component of the magnetic field for an evolution using the modified (eqn. 7) de Sitter metric. In order to make clear that the wave is cleanly passing through $\mathscr{I}^+$ through the course of the evolution, we have multiplied the field by r^2, making the scale of the field comparable at the orgin and at $\mathscr{I}^+$. This can be seen in a more local way in Figure 7, which shows the time evolution of $\mathcal{B}^z$ at a single point on $\mathscr{I}^+$, for four cases. One is the analytic value of the field (in extended Minkowski spacetime) for comparison. Those which fail to keep the field zero after the pulse passes used the two (Minkowski and de Sitter) metrics where the equation (7) modifications to make the grid boundaries beyond $\mathscr{I}^+$ spacelike were not implemented.

Note that the analytic solution is with zero cosmological constant, whereas the numerically evolved solution is with finite cosmological constant, and yet the waveforms coincide. This phenomenon can be understood as follows. Because, as pointed out in II A, the outgoing speed of light is the same in either case, the phase of outgoing waves can be said to be independent of a cosmological constant here. Further, since by construction the initial wave pulse is identical in our Minkowski and de Sitter simulations, by conservation of energy the wave amplitudes at $\mathscr{I}^+$ are expected to be commensurate.

These results show that many desired aims of this approach are achieved. Waves propagate smoothly through $\mathscr{I}^+$ and no difficulties appear to arise in the neighborhood of $\mathscr{I}^+$ The compactified hyperboloidal slices allow waves to appear at $\mathscr{I}^+$ a very short computational time after they originate in the central region. No modifications were needed to integration algorithms designed for conventional spacelike Cauchy slicings. The excision at a cubic computational boundary, however, only maintained acceptable behavior for a time several times the pulse width, and ultimately led to behaviors in the unphysical region beyond $\mathscr{I}^+$ which became intolerabale. An example is given in Fig A2 where the constraint violations beyond $\mathscr{I}^+$ are seen eventually to increase exponentially. In addition, by using analytically constructed initial values satisfying the constraints, we had to accept nonzero initial conditions in the unphysical region $r > 2$ beyond $\mathscr{I}^+$, and the subsequent evolution of these fields complicated the computation beyond $\mathscr{I}^+$.

We believe that further developments of Cauchy evolutions with compactified hyperboloidal slicings and artificial cosmology should be done with the computational/excision boundary a spherical hypersurface at or modestly beyond $\mathscr{I}^+$. The means for doing this have been developed, e.g. [24–27]. Then the possibility remains open that well posed wave equations could run indefinitely. As explained in the supplementary material (Appendix A), we did not here use the differential equations from Section VI of [2] as our lightcone engineering (see Section II A) beyond $\mathscr{I}^+$ makes the constraints there increase exponentially even from analytic arguments. A

spherical boundary could be spacelike at $r > 2$ without the need for such artificial tilting of the lightcones, and thus allow the use of the formulation [2, Equations 26] where constraints evolve causally.

Acknowledgments

This work was supported in part by NASA Space Sciences Grant ATP02-0043-0056. JvM and DRF were also supported in part by the Research Associateship Programs Office of the National Research Council. CWM gratefully acknowledges the hospitality of the AEI, where much of this work was developed.

[1] C. W. Misner, in *DESERFEST: A Celebration of the Life and Works of Stanley Deser*, edited by J. T. Liu, M. J. Duff, K. S. Stelle, and R. P. Woodard (World Scientific, Singapore, 2006), ISBN 981-256-082-3, arXiv:gr-qc/0409073.

[2] C. W. Misner (2005), arXiv:gr-qc/0512167.

[3] C. W. Misner, M. Scheel, and L. Lindblom, *Wave propagation with hyperboloidal slicings* (2003), URL `http://online.kitp.ucsb.edu/online/gravity03/misner`.

[4] S. Husa, in [28], pp. 239–260, arXiv:gr-qc/0204043.

[5] H. Friedrich, in [28], pp. 1–50, arXiv:gr-qc/0209018.

[6] J. Winicour, Living Rev. Relativity **8**, 10 (2005), [Online article]: cited December 22, 2005, `http://www.livingreviews.org/lrr-2005-10`.

[7] J. Frauendiener, Living Rev. Relativity **7**, 1 (2004), [Online article]: cited January 11, 2005, `http://www.livingreviews.org/lrr-2004-1`.

[8] F. Pretorius, Phys. Rev. Lett. **95**, 121101 (2005), arXiv:gr-qc/0507014.

[9] R. Arnowitt, S. Deser, and C. W. Misner, in *Gravitation: An Introduction to Current Research*, edited by L. Witten (Wiley, New York, 1962), pp. 227–265, arXiv:gr-qc/0405109.

[10] B. Brügmann, Phys. Rev. D **54**, 7361 (1996).

[11] D.-I. Choi, J. D. Brown, B. Imbiriba, J. Centrella, and P. MacNeice, J. Comp. Phys. **193**, 398 (2004).

[12] B. Imbiriba, J. Baker, D.-I. Choi, J. Centrella, D. R. Fiske, J. D. Brown, J. van Meter, and K. Olson, Phys. Rev. D **70**, 124025 (2004), arXiv:gr-qc/0403048.

[13] D. R. Fiske, J. G. Baker, J. R. van Meter, D.-I. Choi, and J. M. Centrella, Phys. Rev. D **71**, 104036 (2005).

[14] E. Schnetter, S. H. Hawley, and I. Hawke, Class. Quant. Grav. **21**, 1465 (2004).

[15] U. Sperhake, B. Kelly, P. Laguna, K. L. Smith, and E. Schnetter, Phys. Rev. D **71**, 124042 (2005), arXiv:gr-qc/0503071.

[16] B. Brügmann, W. Tichy, and N. Jansen, arXiv:gr-qc/0312112 (2003).

[17] J. G. Baker, J. Centrella, D.-I. Choi, M. Koppitz, and J. van Meter (2005), arXiv:gr-qc/0511103.

[18] J. G. Baker, J. Centrella, D.-I. Choi, M. Koppitz, and J. van Meter (2006), arXiv:gr-qc/0602026.

[19] D. R. Fiske, Ph.D. thesis, University of Maryland, College Park (2004), `http://hdl.handle.net/1903/1805`.

[20] A. M. Knapp, E. J. Walker, and T. W. Baumgarte, Phys. Rev. D **65**, 064031 (2002), arXiv:gr-qc/0201051.

[21] D. R. Fiske, Phys. Rev. D **69**, 047501 (2004), arXiv:gr-qc/0304024.

[22] S. A. Teukolsky, Phys. Rev. D **61**, 087501 (2000), arXiv:gr-qc/9909026.

[23] D. Shoemaker, K. Smith, U. Sperhake, P. Laguna, E. Schnetter, and D. Fiske, Class. Quant. Grav. **20**, 3729 (2003), arXiv:gr-qc/0301111.

[24] L. E. Kidder, L. Lindblom, M. A. Scheel, L. T. Buchman, and H. P. Pfeiffer, Phys. Rev. **D71**, 064020 (2005), arXiv:gr-qc/0412116.

[25] J. Thornburg, Class. Quant. Grav. **21**, 3665 (2004), arXiv:gr-qc/0404059.

[26] L. Lehner, O. Reula, and M. Tiglio, Class. Quant. Grav. **22**, 5283 (2005), arXiv:gr-qc/0507004.

[27] P. Diener, E. N. Dorband, E. Schnetter, and M. Tiglio (2005), arXiv:gr-qc/0512001.

[28] H. Friedrich and J. Frauendiener, eds., *Tübingen Workshop on the Conformal Structure of Space-times*, Lecture Notes in Physics **604** (Springer, 2002).

APPENDIX A: AUXILIARY MATERIAL

This section is mainly a collection of graphs which illustrate properties that are merely asserted in the main article.

1. Constraints

Even when the modified de Sitter metric is used, the solution in the unphysical region deteriorates as shown in Figs. A1 and A2.

In spite of these problems, the field at $\mathscr{I}^+$ remains zero after the wave pulse passes (Fig. 7) for a moderately long time, which time can be lengthened by using higher resolution. See Fig. A3. Better control of the constraints should be possible using the equation system [2, Equations 26] where the constraints propagate inside the lightcone and damp at a rate $-\partial_i\beta^i$. However this is damping only for the Minkowski or de Sitter metrics as seen in Fig. A4 and becomes anti-damping for our modification of the de Sitter metric (see Fig. A5) which makes our cubic grid boundaries spacelike.

2. Initial conditions beyond $\mathscr{I}^+$.

A second reason which makes the use of the full cubic grid (rather than only a region inside a spherical boundary such as $r = 2$ or $r = 2.1$) inappropriate for numerical computation is the need for initial values beyond $\mathscr{I}^+$ which is $r = 2$ or $R = \infty$.

With a spherical excision boundary and causal propagation of all modes, there is less room for bad initial conditions to intrude, and better reason to think that even poor initial conditions would be quickly flushed out of the computational domain. We have simply used as initial conditions the formulas for $\mathcal{B}$ and $\mathcal{D}$ as computed from equations (12) through (14) extended analytically by the coordinate transformation from $TSYZ$ to $uxyz$ of equations (2). As a solution of the Maxwell equations in the Minkowski metric, these formulae give substantial activity in the $r > 2$ region, as seen in Fig.A6. In that Figure one solution has been modified by smoothly deleting the terms involving $\exp -\lambda V^2$ for $r \geq 2$ which is possible since $V/s = u - 2 + 2/(1 - \frac{1}{2}r)$ becomes infinite at $r = 2$. However the pulse seen moving inward from beyond the grid will have depended upon initial conditions far outside $r = 3.64 = 2.1\sqrt{3}$ which was the limit of our grid. Our initial data, however, are not evolved using the Minkowski metric, but usually with the de Sitter or modified de Sitter metrics, where the decomposition into ingoing and outgoing parts of the initial conditions will differ seriously from the Minkowski case, especially well beyond $\mathscr{I}^+$. Thus we can understand that different, but equally visible, activity could occur in the $r > 2$ region which would be actually solving the given differential equations but be unrelated to the physical activity in the region $r \leq 2$. This appears to be occuring in the numerical results (modified de Sitter for which no analytic solution is available) shown in Fig. A7.

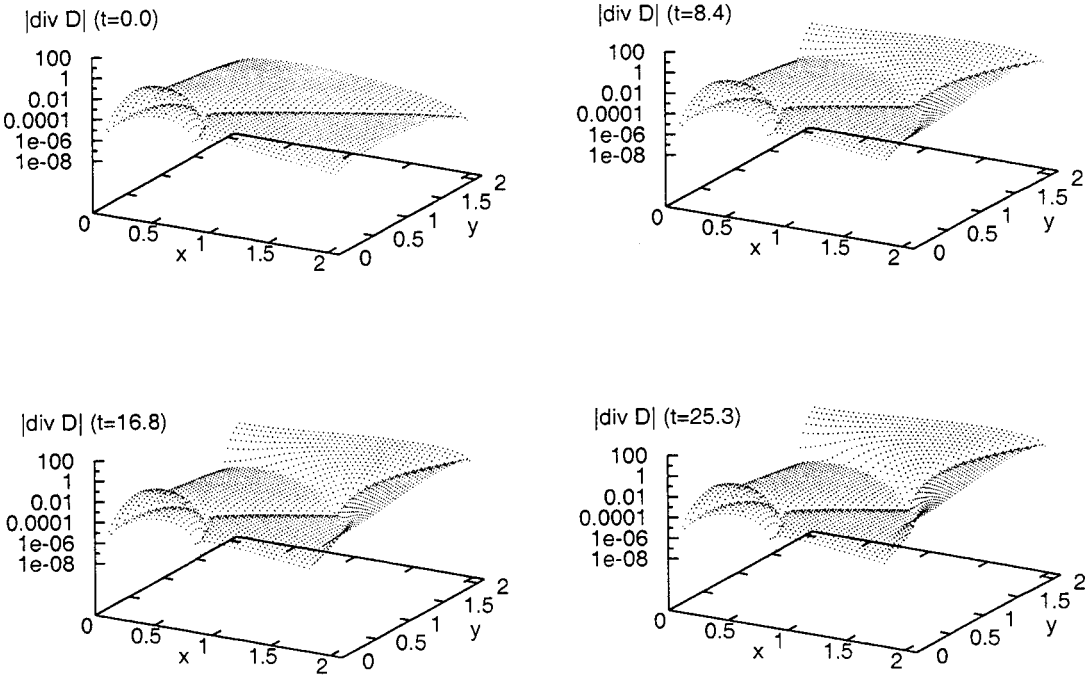

FIG. A1: Samples of the time evolution of the constraint violation $|\mathrm{div}\mathcal{D}|$ at $z = 0$ within our comptational cube $|x^i| < 2.1$ whose edges are at $r = 2.97$.

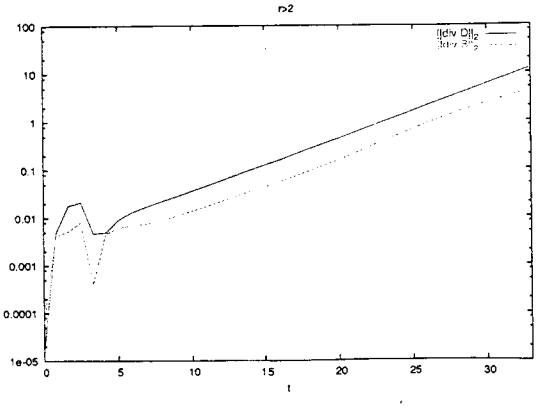

FIG. A2: The time evolution of an L2 norm of the constraint violations over the unphysical region $r > 2$ beyond $\mathscr{I}^+$ within our computational cube $|x^i| < 2.1$ whose corners are at $r = 3.64$.

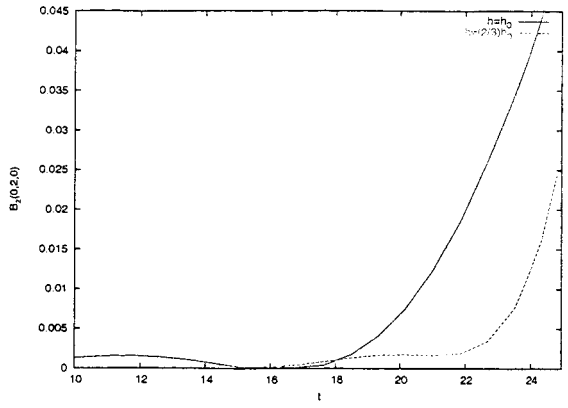

FIG. A3: A continuation of the test wave pulse to later times at $\mathscr{I}^+$.

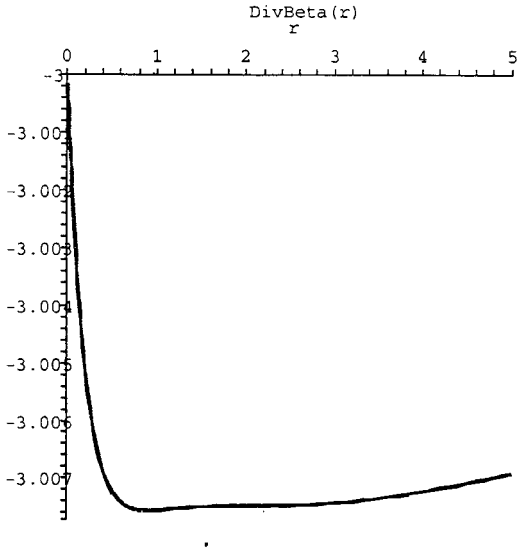

FIG. A4: The damping factor for constraints in the de Sitter metric.

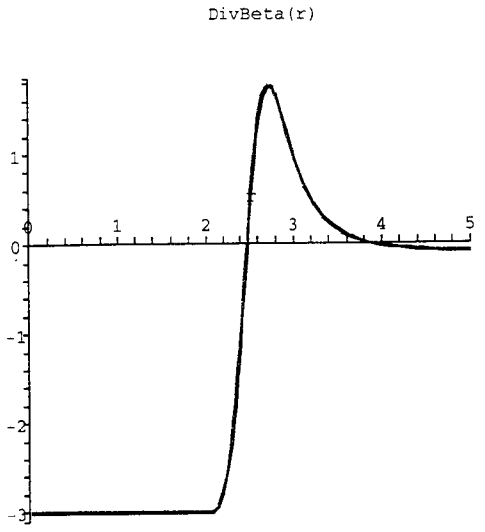

FIG. A5: The damping factor for constraints in the modified de Sitter metric. Where divβ is positive, the constraints should grow exponentially at the plotted e-folding rate.

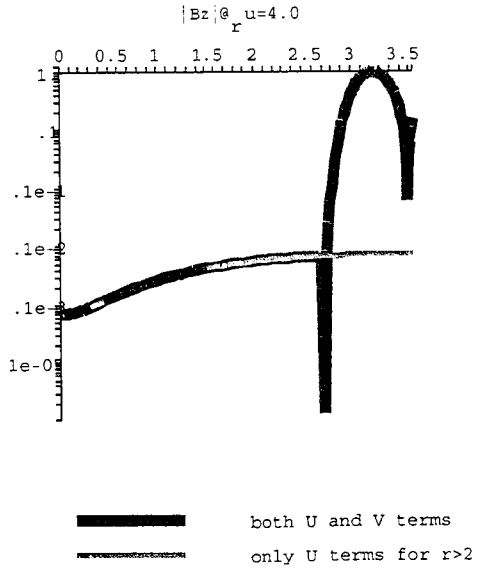

FIG. A6: For the analytic solution in Minkowski spacetime: The magnetic field at $z = 0$ after the pulse from Fig 7 has exited the computational grid.

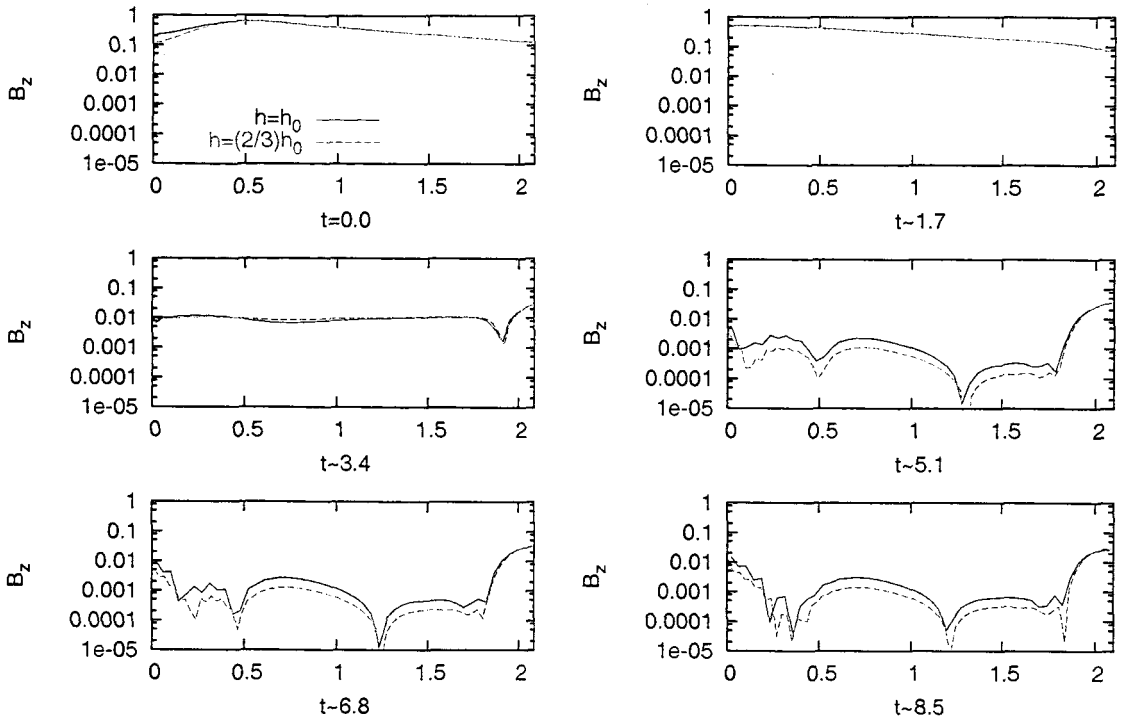

FIG. A7: A field component plotted along a line $z = 0, x = 1$ parallel to the y-axis. At the grid limit $y = 2.1$ one has $r = 2.33$, while $\mathscr{I}^+$ is met at $y = 1.73$. Inside $\mathscr{I}^+$ the field values appear to be convergent to zero after $u = 4$, while in the region beyond $y = 1.85$ or $r = 2.1$ a slowly moving pulse appears to remain independent of the selected resolution.